

## Numerical solution of the Boltzmann equation in cylindrical geometry

G.J. Parker,<sup>1</sup> W.N.G. Hitchon,<sup>2</sup> and J.E. Lawler<sup>1</sup>

<sup>1</sup>*Department of Physics, University of Wisconsin, Madison, Wisconsin 53706*

<sup>2</sup>*Electrical and Computer Engineering Department and Engineering Research Center for Plasma Aided Manufacturing, University of Wisconsin, Madison, Wisconsin 53706*

(Received 4 February 1994; revised manuscript received 3 June 1994)

A numerical procedure that provides an accurate solution of the Boltzmann equation in cylindrical geometry with coordinates  $(\rho, \vec{v})$  is discussed. Statistical methods such as Monte Carlo can be used but suffer from statistical noise and thus do not resolve low density regions well. Furthermore, the slow speed of pure Monte Carlo methods makes self-consistent simulations quite difficult. A direct solution of the Boltzmann equation avoids these difficulties but suffers from errors due to finite size mesh effects. In this work we examine a solution method, based on the convected scheme, that eliminates some specific sources of numerical diffusion in cylindrical geometry. The velocity is represented as  $(v_z, v_\perp, \mathcal{M})$ , where  $\mathcal{M}$  is a moment arm or “reduced” angular momentum,  $\mathcal{M} = \rho \sin \phi$ , and  $\phi$  is an azimuthal angle in velocity space (referenced to the unit vector  $\hat{\rho}$ ). The reasons for all the coordinate choices are discussed. Propagator algorithm(s) for solving the kinetic equation are presented which remove certain numerical errors. Examples of the performance of the algorithm(s) under various conditions are presented and discussed. A self-consistent kinetic model of a dc positive column is described.

PACS number(s): 02.70.Rw, 05.20.Dd, 52.65.+z

### I. INTRODUCTION

We present a scheme for solution of the kinetic equation in one spatial variable, the cylindrical radius  $\rho$ , and three components of velocity,  $\vec{v}$ . It is a version of the “convected scheme” (CS) [1–4] which provides a fully self-consistent and kinetic treatment of the positive column discharge. In a CS simulation the electron distribution function  $f_e(\vec{r}, \vec{v}, t)$  (as well as the ion distribution function) is advanced in time using a propagator

$$f_e(\vec{r}, \vec{v}, t + \Delta t) = \int \int f_e(\vec{r}'', \vec{v}'', t) \times p(\vec{r}, \vec{v}, \vec{r}'', \vec{v}'', \Delta t) d^3 r'' d^3 v''. \quad (1)$$

The propagator (or Green’s function) is broken into two parts: ballistic motion followed by collisions. The distribution functions and propagators are defined on a phase space mesh. The simultaneous solution of Poisson’s equation makes the simulation self-consistent.

In earlier work we have implemented an algorithm based on the method of characteristics that avoids certain sources of errors in finding the distribution function. It does not use interpolation to implement the method of characteristics so there is no assumption of “smoothness” or that derivatives are well defined everywhere. It also is set up to exactly conserve particles and energy locally on the mesh [1–3]. Since it uses characteristics it can take long time steps, which reduces the number of steps and decreases the errors associated with each step. Tests of the method have been described elsewhere [1–3]. In extending this approach to cylindrical geometry, new sources of error arise. We show below how we can design a mesh and a solution scheme in cylindrical geometry which has the advantages of the schemes we developed in previous work.

In the past, we modeled dc and rf glow discharges between parallel plate electrodes, using the variables  $(z, v_z, v_\perp)$  [1–3], where  $z$  is the distance from one electrode,  $v_z$  is the corresponding velocity component, and  $v_\perp$  is the magnitude of the velocity component perpendicular to the  $z$  axis. Both the phase space mesh and propagators must be redefined in order to perform simulations in cylindrical geometry. The spatial coordinate  $z$  is replaced by a radial spatial coordinate  $\rho$  and a third velocity coordinate is added to provide a representation of the two components of  $v_\perp$ . The separability of  $v_z$  from  $\rho$  and from the components of  $\vec{v}$  in the azimuthal plane makes this a useful choice.

The perpendicular velocity is represented by its magnitude  $v_\perp$  and by  $\mathcal{M} = \rho \sin \phi$ , where  $\rho$  is the (spatial) cylindrical radius and  $\phi$  is an azimuthal angle made by the velocity  $\vec{v}$  with respect to  $\hat{\rho}$  in the azimuthal plane. The magnitude of the angular momentum per unit mass about the  $z$  axis ( $\rho = 0$ ) is then  $\mathcal{M}v_\perp$ . Reasons for using  $v_\perp$  and  $\mathcal{M}$  instead of  $v_\rho$  and  $v_\phi$  are discussed in Sec. II.

In this paper, we first describe the coordinate system and the mesh we use for electrons in cylindrical geometry (Sec. II). Section III treats the “ballistic move” of the electrons on this mesh; Sec. IV deals with collisions of electrons with neutral atoms. Section V treats the ballistic move of ions on a related but simplified mesh in cylindrical geometry. Section VI describes ion-atom collisions. Section VII presents tests of the algorithms.

### II. COORDINATE SYSTEM AND MESH FOR ELECTRONS IN CYLINDRICAL GEOMETRY

In this section, the coordinate system used to describe electron motion is described, as well as the reasons for choosing it. Then the electron mesh is introduced.

In earlier work on discharges between parallel plate electrodes, two different coordinate systems were used to describe electron motion;  $(z, v, \mu)$  and  $(z, v_z, v_\perp)$  [1-4]. In this earlier work  $z$  was the spatial coordinate (distance from one of the infinite plane parallel electrodes),  $v_z$  is the corresponding velocity,  $v$  is the total speed,  $\mu \equiv v_z/v$ , and  $v_\perp$  is the speed in the plane perpendicular to  $z$ .

Collisions are easier to describe in the set  $(z, v, \mu)$ , because we often know the final energy after a collision, hence  $v$ , and need to distribute scattered electrons to various  $\mu$ . It is relatively easy in this case to distribute the scattered electrons on the  $(z, v, \mu)$  mesh. If the final  $v$  after the collision is equal to the initial  $v$ , it can be done with no numerical diffusion in  $v$ . Isotropic scattering of electrons results in a uniform distribution in  $\mu$ .

On the other hand, the set  $(z, v_z, v_\perp)$  is better suited to describe the ballistic motion. All the cells at different  $v_\perp$  but having the same  $(z, v_z)$  have the same ballistic motion, and this can be exploited to accelerate the "move" [1]. Collisions are more difficult using  $(z, v_z, v_\perp)$ . If the speed after the collision equals the speed before, but the angle is different, it will usually not be possible to find a cell with the exact  $v$ . Then the electrons must be split between two or more cells, to conserve energy. A "simplified" elastic collision operator, which conserves energy but is "grainy" in polar angle, was developed to reduce numerical diffusion (in kinetic energy) and speed up the calculation [2,5]. The simplified elastic collision operator removes the most severe problem due to numerical diffusion in the set  $(z, v_z, v_\perp)$  and preserves the advantages of the set of variables during ballistic moves.

Extending the calculation to include the radial motion is more straightforward when based on the  $(z, v_z, v_\perp)$  set than  $(z, v, \mu)$ , because the ballistic motion is less coupled in the former case. Collisions present no substantial difficulties in either case, although some care is necessary. The mesh for  $v_\perp$  is the same as the  $v_z$  mesh but independent of  $v_z$ . The radial motion is then the same for all values of  $v_z$  that share those components of  $v_\perp$ . If we used  $(v, \mu)$  and some other variable such as  $\phi$ , the azimuthal

angle in velocity space, the radial motion would be different for every permutation of the values of  $(v, \mu, \phi)$  on the mesh. This would greatly increase the computational difficulty.

Having established the reason for using  $v_z$  and components of  $v_\perp$ , we now turn to the components of  $v_\perp$ . The set we choose is  $(v_\perp, \mathcal{M})$ , where  $v_\perp$  is the magnitude of the velocity component perpendicular to the  $z$  axis ( $\rho = 0$ ) and  $\mathcal{M} \equiv \rho \sin \phi$ . Here  $\rho$  is the radius,  $\phi$  is an azimuthal angle between the velocity and  $\hat{\rho}$ , and thus  $\mathcal{M}$  is a moment arm or a "reduced" angular momentum. The magnitude of the angular momentum about the  $z$  axis ( $\rho = 0$ ) is  $v_\perp \mathcal{M}$ , but if we work with  $\mathcal{M}$ , the  $\mathcal{M}$  mesh is independent of  $v_\perp$ .

The choice to use  $\mathcal{M}$  is partly because it is a conserved quantity during the ballistic motion (in the case of zero radial electric field). More importantly, however, a mesh in  $(v_\rho, v_\phi)$  leads to unacceptable numerical diffusion. As electrons move radially outward in  $\rho$  in the absence of an electric field, the angle  $\phi$  decreases (where  $\phi$  is defined to be zero for an electron moving purely radially outwards). Electrons in the smallest  $\phi$  cell at one radius should be placed in a smaller  $\phi$  cell at the next radius they go to. On a uniform  $\phi$  mesh this is impossible, unless there is a cell at  $\phi = 0$ . A cell at  $\phi = 0$  will then trap electrons at  $\phi = 0$  if they bounce off the outer wall and move to smaller radii. In either case, electrons are "pumped" towards or away from  $\phi = 0$ . Numerical diffusion then becomes a severe problem.

The way to avoid this systematic inaccuracy is to choose a mesh on which cells from one radius are mapped exactly onto cells at all other radii (at least when the radial electric field is zero). This essentially means using  $\mathcal{M}$  to define the mesh. The  $\mathcal{M}$  mesh has two distinct parts, one for electrons with negative radial velocities (inward going) and one with positive radial velocities (outward going). Figure 1 is an illustration of the mesh in the  $(\rho, \mathcal{M})$  plane. The halves of the mesh share a single  $\mathcal{M}$  cell at the smallest radius. The innermost cell is labeled " $a_0$ " in Fig. 1 and it includes  $\rho$  values from 0 to  $\rho_1$  and

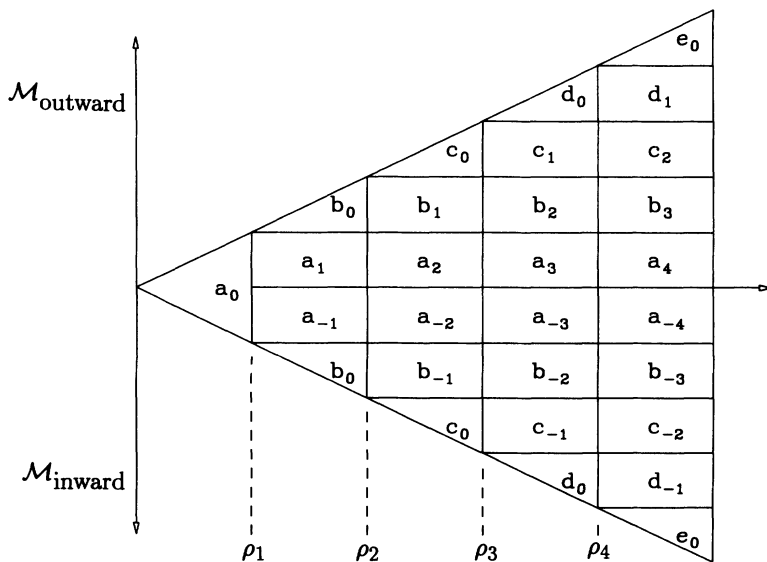


FIG. 1. Schematic of  $(\rho, \mathcal{M})$  mesh. With  $E_\rho = 0$ , particles will travel horizontally. For example, starting at  $b_{-2}$ , a particle will travel to  $b_{-1}$ ,  $b_0$ ,  $b_1$ ,  $b_2$ , . . .



of the electrons will leave the  $b_2$  cell. A fraction  $(\Delta\eta_{b_2} - \sum_{n=3}^{q-1} \eta_{b_n})/\eta_{b_2}$  of the electrons from cell  $b_2$  will reach cell  $b_q$  where  $0 < \Delta\eta_{b_2} - \sum_{n=3}^{q-1} \eta_{b_n} < \eta_{b_q}$ . Cell  $b_q$  is the furthest cell reached by electrons from  $b_2$  during  $\Delta t$ . The remaining electrons are distributed in sequence to the  $b_{q-1}, b_{q-2}, \dots$  cells. The fraction of the electrons distributed to the  $b_{q-r}$  cell is the lesser of the fraction remaining or  $\eta_{b_{q-r}}/\eta_{b_2}$ .

When a radial electrostatic potential  $\Phi(\rho)$  is included, the above algorithm is slightly adjusted to take into account the radial force. The equation of motion for  $v_\perp$  is

$$\dot{v}_\perp = \pm \frac{e}{m} \frac{\partial \Phi(\rho)}{\partial \rho} (1 - \mathcal{M}^2/\rho^2)^{1/2}, \quad (8)$$

where the minus sign is used for inward going electrons. During the computation of  $\Delta\eta$  using Eq. (6),  $(v_{\perp,j}^3 - v_{\perp,j-1}^3)/3$  is approximated as  $\overline{v_{\perp,j}}(v_{\perp,j}^2 - v_{\perp,j-1}^2)/2$ , where

$$\overline{v_{\perp,j}} = \overline{v_{\perp,j}} \mp \frac{e}{2m} E_\rho (1 - \overline{\mathcal{M}_k^2/\bar{\rho}_i^2})^{1/2} \Delta t. \quad (9)$$

The error in this approximation decreases with decreasing mesh size; the error vanishes for an infinitesimal mesh. The above equation defines a time average  $v_\perp$  during  $\Delta t$ . For an initial cell, the volume of phase space "swept-out" is computed for each radial boundary by using  $E_\rho$  at each boundary. This allows the initial phase space volume to expand or contract in the radial direction.

Using this time average  $v_\perp$  during  $\Delta t$  simplifies the phase space volume calculations. Specifically, the only variables that enter into the phase space volumes are  $\rho$  and  $\mathcal{M}$  (or correspondingly  $\phi$ ).

Conservation of energy is used to update the distribution in  $v_\perp$ . Suppose some of the electrons from the initial cell with mean radius  $\bar{\rho}_i$  and mean velocity  $\overline{v_{\perp,j}}$  are distributed to a final spatial cell with mean radius  $\bar{\rho}_m$ . These electrons should, by conservation of energy, have a moved perpendicular velocity,  $v'_\perp$ , given by

$$v'_\perp = \left( \overline{v_{\perp,j}^2} + \frac{2e}{m} [\Phi(\bar{\rho}_m) - \Phi(\bar{\rho}_i)] \right)^{1/2}. \quad (10)$$

Typically  $v'_\perp$  does not correspond exactly to the mean  $v_\perp$  in a cell on the mesh, in which case the electrons are shared between the two neighboring  $v_\perp$  cells in such a way that kinetic energy (in the azimuthal plane) is conserved. If a final radial spatial cell is energetically forbidden, the electrons retrace their trajectory to the previous radial cell, reversing the sign of their radial velocity.

Once  $\rho$  and  $v_\perp$  distributions are updated, the  $\mathcal{M}$  distribution must be updated. The electrons distributed to a final cell with mean values  $\bar{\rho}_m$  and  $\overline{v_{\perp,n}}$  have a moved  $\mathcal{M}$  given by

$$\mathcal{M}' = \frac{\overline{v_{\perp,j}} \overline{\mathcal{M}_k}}{\overline{v_{\perp,n}}}. \quad (11)$$

Again, typically  $\mathcal{M}'$  is not exactly equal to the mean  $\mathcal{M}$  in a cell on the mesh, in which case the neighboring  $\mathcal{M}$  cells are used as final cells. Due to the discreteness of

the  $v_\perp$  mesh, the above equation may give a  $\mathcal{M}'$  which is outside the allowed range (at that spatial location). In this case, the electrons retrace their trajectories to the previous radial cell (reversing the sign of the radial velocity).

Complete decoupling of the  $z$  motion from the radial motion results in a very simple ballistic mover for  $v_z$ . The axial field  $E_z$  is uniform in a positive column. The  $(i, j, k, l)$  initial cell has mean velocity  $\overline{v_{z,l}}$ . After a time step  $\Delta t$ , the moved cell has

$$v'_z = \overline{v_{z,l}} - eE_z \Delta t/m. \quad (12)$$

This moved velocity is typically not equal to the mean  $v_z$  in a cell on the mesh. The two neighboring cells are chosen and the fraction going to each of these final cells is determined so that the energy  $(mv_z^2/2)$  is conserved.

#### IV. THE ELECTRON COLLISION OPERATOR

Cross sections for electron-atom (and ion-atom) collisions in helium are better known than those for any other gas. Simulations reported here, like most of our earlier simulations, are for He glow discharges in order to facilitate meaningful comparisons with experiments.

Elastic electron-atom collisions, inelastic collisions resulting in excitation, and inelastic collisions resulting in single-step ionization are included in the electron collision operator, as well as Coulomb collisions between electrons.

Two versions of the elastic collision operator are used. The "simplified" version includes momentum transfer but neglects energy transfer due to recoil during electron-atom collisions. The simplified operator is also "grainy" in its angular distribution. The primary advantage of the simplified operator is that it is free from numerical diffusion in kinetic energy. High rates of elastic scattering can otherwise result in significant numerical diffusion in energy.

The full elastic scattering operator is used after, say, 499 operations of the simplified operator. It includes extra energy loss due to recoil to compensate for neglecting recoil energy loss in the simplified operator. The full operator also has a smoother angular redistribution of scattered electrons.

Both operators have been designed to provide an isotropic distribution of scattered electrons with a scattering rate computed from the elastic momentum transfer cross section, or to provide an anisotropic distribution with a scattering rate computed from the total elastic cross section. The following describes the implementation of the momentum transfer (isotropic) approximation. A momentum transfer cross section  $\sigma_{MT}$  is determined from LaBahn and Callaway's differential elastic scattering cross section [7]. The fraction,  $N_{\text{scatt}}/N_{\text{cell}}$ , of electrons elastically scattered out of a cell with indices  $(i, j, k, l)$  during a time step  $\Delta t$  is

$$N_{\text{scatt}}/N_{\text{cell}} = \sigma_{MT} (\overline{v_{z,l}^2} + \overline{v_{\perp,j}^2} + 3k_B T_g/M)^{1/2} N \Delta t, \quad (13)$$

where  $k_B$  is Boltzmann's constant,  $T_g$  is the gas tempera-

ture,  $M$  is the mass of a He atom, and  $N$  is the density of He atoms. The full operator redistributes the scattered electrons with a reduced kinetic energy

$$(v')^2 = \bar{v}_{z,l}^2 + \bar{v}_{\perp,j}^2 - \frac{4}{M} \left( \frac{m}{2} (\bar{v}_{z,l}^2 + \bar{v}_{\perp,j}^2) - \frac{3}{2} k_B T_g \right). \quad (14)$$

Isotropic redistribution is accomplished by putting a fraction,  $(v_{z,p} - v_{z,p-1})/v'$ , of the scattered electrons into the  $p$ th  $v_z$  cell for all  $|v_{z,p}| < v'$ . The corresponding  $v_{\perp}$  cell(s) are at

$$v'_{\perp} = [(v')^2 - \bar{v}_{z,p}^2]^{1/2}. \quad (15)$$

Usually the absence of a  $v_{\perp}$  cell at this precise  $v'_{\perp}$  requires splitting the electrons between two adjacent cells in a fashion which conserves energy. Isotropic redistribution on the  $\mathcal{M}$  mesh requires that the fraction of the scattered electrons distributed to the  $q$ th cell on the  $\mathcal{M}$  mesh be proportional to the range  $\Delta\phi$  of  $\phi$  in the cell;

$$\Delta\phi_q \equiv \phi_q - \phi_{q-1} = \sin^{-1} \left( \frac{\mathcal{M}_{q+1}}{\bar{\rho}_i} \right) - \sin^{-1} \left( \frac{\mathcal{M}_q}{\bar{\rho}_i} \right). \quad (16)$$

The simplified elastic scattering operator redistributes electrons among a subset of cells which have different values of  $v_z$  and  $v_{\perp}$  but have exactly the same total kinetic energy. The simplified operator is quite similar to that described previously and used during simulations in the variables  $(z, v_z, v_{\perp})$  [2,5]. The only significant refinement is that both the full and simplified operators provide a complete redistribution (uniform in  $\phi$ ) on the  $\mathcal{M}$  mesh.

Cross sections for excitation to singlet and triplet He  $s, p,$  and  $d$  levels with principal quantum numbers  $n = 2, \dots, 5$  are taken from Alkhazov [8]. The kinetic energy of the scattered electrons is

$$mv'^2/2 = m(\bar{v}_{z,l}^2 + \bar{v}_{\perp,j}^2)/2 - \tau_r, \quad (17)$$

where  $\tau_r$  is the threshold energy for the  $r$ th inelastic process. Isotropic angular distributions are achieved using the same algorithm as in elastic scattering.

The cross section for electron impact ionization is also from Alkhazov [8]. The two outgoing electrons from single-step ionization share the available energy according to the differential cross section [8]. Isotropic angular distributions for the ejected and scattered electrons are achieved using the same algorithm as in elastic scattering.

For an anisotropic redistribution of scattered particles, scattered particles are assumed to have a distribution given by a two-term Legendre polynomial. To find the coefficients of each term, number and an average  $v_z$  are conserved. Electrons are still redistributed isotropically in  $\mathcal{M}$  space. The anisotropic distribution is described in the appendix, and is necessary for an accurate computation of the  $v_z$  distribution [2,5]. Electron-electron Coulomb collisions are also included in an approximate manner to describe energy transfer between electrons. The algorithm used here is identical to that described in Ref. 5.

## V. THE ION BALLISTIC MOVE

In this section, we describe how the ballistic motion of the ions is implemented numerically. Unlike electrons, the ions are adequately described using  $(\rho, v_{\rho}, v_z)$  for cylindrical geometry, where  $v_{\rho}$  is the component of the velocity in the radial direction. The remaining component of velocity at the beginning of a ballistic move is assumed to be given by a Maxwellian distribution at the neutral gas temperature. This approximation is adequate if the mean free path for charge-exchange collisions with neutral atoms is comparable to or less than the radial “width” of the cell. This approximation is related to a “cold gas” approximation in which the ions move radially outward in a positive column. Both approximations avoid tracking any ion angular momentum about the  $z$  axis. Our approximation, of setting  $v_{\phi} = \sqrt{k_B T_g/M}$  at the beginning of the ballistic move, provides a small centrifugal acceleration. This acceleration helps prevent ions from “piling up” in the innermost radial cell.

Ion ballistic motion is described by solving the equations of motion. We will discuss motion in the azimuthal plane without and then with a radial electric field. The  $v_z$  distribution is updated in exactly the same way the electron  $v_z$  distribution is updated.

The initial cell with indices  $(i, j, k)$  has mean values of the coordinates given by  $\bar{\rho}_i, \bar{v}_{\rho,j},$  and  $\bar{v}_{z,k}$ . It has faces at  $\rho_{i-1}, \rho_i, v_{\rho,j-1}, v_{\rho,j}, v_{z,k-1}, v_{z,k}$ , where  $\bar{\rho}_i = (\rho_{i-1} + \rho_i)/2, \dots$ , as before. We approximate the initial  $v_{\phi} \equiv \sqrt{k_B T_g/M}$ . The equation of motion for the radial coordinate is

$$\ddot{\rho} = \frac{L^2}{M^2 \rho^3} + \frac{e}{M} E_{\rho}(\rho) \quad (18)$$

where  $L$  is the angular momentum about the  $z$  axis and  $M$  is the mass of the ion. The angular momentum  $L$  is conserved; at the start of a move  $L = M\rho\sqrt{k_B T_g/M}$ . Note that  $(v_{\rho}^2 + v_z^2)$  is also conserved when  $E_{\rho} = 0$ . The mover is constructed from the exact solution of this equation in the  $E_{\rho} = 0$  limit. The second integral with  $E_{\rho} = 0$  yields

$$[\rho(t + \Delta t)]^2 = [\rho(t)]^2 + 2\rho(t)v_{\rho}(t)\Delta t + \{k_B T_g/M + [v_{\rho}(t)]^2\}\Delta t^2. \quad (19)$$

The location of the moved cell face  $\rho'_i$  is

$$(\rho'_i)^2 = (\rho_i)^2 + 2\rho_i \bar{v}_{\rho,j} \Delta t + (k_B T_g/M + \bar{v}_{\rho,j}^2)\Delta t^2. \quad (20)$$

The direction the cells are moving is determined by the sign of  $v_{\rho}$ . Both radial faces of the cell are moved independently.

When a radial electrostatic potential  $\Phi(\rho)$  is included, the above algorithm is slightly adjusted to take into account the radial force. The equation of motion for  $v_{\rho}$  is

$$\dot{v}_{\rho} = \frac{L^2}{M^2 \rho^3} + \frac{e}{M} E_{\rho}(\rho). \quad (21)$$

During the calculation of the location of the moved radial face using Eq. (20),  $\bar{v}_{\rho,j}$  is replaced by the time average  $v_{\rho}$  during  $\Delta t$ .

$$\overline{v}_{\rho,j} = \bar{v}_{\rho,j} + \frac{L^2}{2M^2\bar{\rho}_i^3}\Delta t + \frac{e}{2M}E_\rho(\bar{\rho}_i)\Delta t. \quad (22)$$

The fraction of the area of the moved cell overlapping each final spatial cell is set equal to the fraction of the ions from the moved cell distributed to each final cell. The velocity of the moved cell is approximately given by equation of motion for  $v_\rho$ ,

$$v'_\rho = \bar{v}_{\rho,j} + \frac{L^2}{M^2\bar{\rho}_i^3}\Delta t + \frac{e}{M}E_\rho(\bar{\rho}_i)\Delta t. \quad (23)$$

Typically,  $v'_\rho$  does not correspond exactly to the mean  $v_\rho$  in a cell on the mesh, in which case the ions are shared between the two neighboring  $v_\rho$  cells in such a way that the moved velocity is conserved.

## VI. THE ION COLLISION OPERATOR

In this section, we describe the ion collision operator. In discharges considered here, ion motion is dominated by charge-exchange collisions with ground state atoms. Cross sections for charge-exchange ( $\sigma_{\text{EX}}$ ) are given by Sinha, *et al.* [9] The cross section is increased slightly to reproduce measured ion mobilities [10], and thereby include the effect of elastic scattering at lower energies.

In a time step  $\Delta t$  the fraction of ions suffering a collision is given by

$$N_{\text{scatt}}/N_{\text{cell}} = \sigma_{\text{EX}} \left( \bar{v}_{z,k}^2 + \bar{v}_{\rho,j}^2 + \frac{4k_B T_g}{M} \right)^{1/2} N \Delta t. \quad (24)$$

The scattered ions are distributed with a Maxwellian distribution at the neutral gas temperature.

## VII. PRELIMINARY TESTS OF THE ALGORITHMS

In this section, we describe some preliminary tests of the electron mover including: (A) verifying that an initially uniform electron distribution in phase space remains uniform, (B) verifying that the density is proportional to  $1/\rho$  when electrons launched in a single radial location are moving only radially outwards (inwards), and (C) verifying that the electrons orbit the  $z$  axis ( $\rho = 0$ ) in simple harmonic and Coulomb potentials.

### A. Initially uniform distribution

This test was designed to help validate the ballistic part of the electron mover by verifying conservation of phase space volume. The simulation was started with the mesh containing a spatially uniform density, at one specific  $v_\perp$ , and isotropically distributed in  $\mathcal{M}$ . No electric field was applied, however, the electrostatic potential  $\Phi$  was discontinuous at  $\rho = \rho_{\text{max}}$ , so that all the electrons would reflect at the outer radius. Regardless of the time step taken and the total time of the simulation, the density remained uniform throughout the column to better than 1 part in 10 000.

### B. Beam distributions and sources

A constant production rate (number per unit time) was introduced at the center cell in this test. Electrons were produced at a specific  $v_\perp$  and directed towards the outer wall. Electrons were allowed to escape at the wall. Again, there was no electric field. When the simulation achieved steady state, the (real-space) density varied as  $1/\rho$  (to within 1%).

In a related test, a source rate was introduced in each radial cell which introduced the same number of electrons per unit time, which corresponds to a production rate per unit volume proportional to  $1/\rho$ . Newly created electrons were all at the same speed and directed towards the radial wall. The steady-state (real-space) density was found to be uniform.

### C. Harmonic and Coulomb potentials

A radial electric field  $E_\rho(\rho)$  was introduced in these tests. The field  $E_\rho(\rho)$  took two forms, namely an harmonic force ( $E_\rho \propto \rho$ ) and a Coulomb force ( $E_\rho \propto 1/\rho$ ) law. After choosing an initial radius and the form of  $E_\rho(\rho)$ , a  $v_\perp$  was found so that the electrons would travel in a circular orbit. The electrons were then launched with their velocity perpendicular to the radial vector. Regardless of the time step  $\Delta t$  and the length of the simulation for these  $E_\rho(\rho)$ , the electrons stayed in the initial radial cell with no diffusion.

Next, the electrons' speed was decreased slightly so that their radial motion should be bounded by the initial radius and a radius three cells nearer the center. Initially a fraction, depending on the time step, of the electrons stayed in the initial cell and the rest moved inwards. About 5% of the electrons, when they first reflected from the centrifugal potential, went past the inner bound. Then as the electrons returned to the initial radius, some (3%) went outward past the initial radial cell. Much later in the simulation, after  $\sim 50$  orbits, the electrons were spread throughout the column, though the majority were still confined to the "physical" region. The reason for this unphysical behavior is numerical diffusion in speed or kinetic energy. As the electrons moved to different radial cells, the mover split the electrons into  $v_\perp$  cells which were too low or high in order to conserve energy on average. This diffusion in energy effectively changes the physical turning points.

### D. Positive column results

Here we show some results for a positive column in helium. The results are preliminary, and cannot yet be compared to highly detailed experiments, because metastable atoms and the associated multistep ionization processes are not yet included in the code. There is only direct ionization from the ground state of helium. The parameters of the discharge are summarized in Table I.

The axial electric field  $E_z$  delivers power to the electrons to sustain the discharge. It was found that simply specifying a fixed value of  $E_z$  caused the simulation to become unstable: too high an  $E_z$  caused the plasma den-

TABLE I. Discharge parameters.

Quantity	Value	Units
Neutral density	1.61	$10^{16} \text{ cm}^{-3}$
Neutral temperature	300	K
$V_0 - V_c$	2.559	kV
$R_B$	200	$\text{k}\Omega$
$L$	13	cm
$\rho_{\text{max}}$	1	mm

sity to increase without bound, too low a value did not sustain the discharge. We then incorporated an external circuit on the discharge, specifying an “effective” applied voltage  $V_0 - V_c$  and ballast resistor  $R_B$ . The supply voltage  $V_0$  and  $V_c$  is the voltage drop across the cathode fall; both are assumed to be constant. The axial electron current is  $I$ . Given the length  $L$  of the positive column, the axial field is given by

$$E_z = \frac{V_0 - V_c - IR_B}{L} \quad (25)$$

and is independent of the radial coordinate.

Gauss’s law is used to compute the radial electric field  $E_\rho(\rho)$ . By symmetry,  $E_\rho(\rho) = 0$  at  $\rho = 0$ . The radial electrostatic potential is found by integrating  $E_\rho(\rho)$ . For convenience,  $\Phi(\rho) = 0$  at  $\rho = 0$ .

Ions hitting the outer radial boundary are assumed to be neutralized and recycled as atoms. Electrons which reach the outer radial boundary are absorbed on the boundary. The wall potential decreases until the flux of electrons to the wall matches the ion flux in steady state. Although we here assume a reflection coefficient of zero for the electrons at the radial boundary, we could just as easily use any value from zero to near unity. The main result of using a (perhaps more physically correct) nonzero reflection coefficient is a smaller radial field.

The simulation, after an external circuit equation including a ballast resistor was introduced, ran stably and quickly. Convergence of the solution was confirmed when the total number of ions per second from direct ionization equaled the number of ions per second hitting the radial boundary to better than 0.5%. A steady-state axial current of 9.93 mA was found. The axial field  $E_z$  fluctuates in steady state by about 5% around 48.2 V/cm, which is larger than the experimental value of 41 V/cm at 10 mA [11]. The difference is in part due to the neglect of multistep ionization in this simulation.

Figure 3 shows the calculated radial electric field  $E_\rho$  and the corresponding potential  $\Phi(\rho)$  as functions of radius.

Figure 4 shows the ion and electron densities as functions of radius. The ion density exceeds the electron density everywhere. Also shown is the average electron energy, which rises toward the outside. It is interesting to note that it is necessary, at these parameters, to include anisotropic scattering of electrons, or some electrons run away near  $\rho = 0$  leading to a peak in the average electron energy near  $\rho = 0$ .

The average electron energies shown in Fig. 4 are quite high. The difference between  $\frac{2}{3}\langle mv^2/2 \rangle_e$  and  $\langle mv^2_{\perp}/2 \rangle_e$

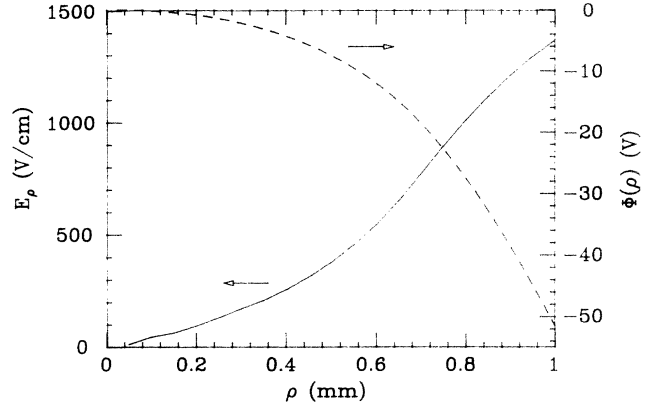


FIG. 3. Radial field  $E_\rho(\rho)$  (solid) and electrostatic potential  $\Phi(\rho)$  (dashed) as functions of  $\rho$ .

is an indication of the anisotropy of the electron velocity distribution. Both observations are consistent with the rather high axial  $E_z/N$  of  $3.0 \times 10^{-15} \text{ V cm}^2$  in the positive column simulation. We deliberately chose a small radius-pressure product of 0.05 cm Torr, which produced the high  $E_z/N$ , in order to accentuate kinetic effects in this first positive column simulation.

Figure 5 shows the ionization rate per unit volume and radial ion flux density as functions of radius. Figure 6 shows the ionization rate as a function of radius.

The classic models of the positive column by Schottky [12] and by Tonks and Langmuir [13] and most subsequent variations assume an electron velocity distribution function that is independent of radius. One of the most interesting results from our kinetic simulations is the radial variation of the electron distribution function. Although there are some earlier models and simulations that explore such radial variations, none of these are for conditions directly comparable to ours. Qualitative, but not quantitative, comparisons are, therefore, appropriate.

Bernstein and Holstein [14] used a spatially averaged two-term Legendre expansion of the electron distribution function to study the influence of radial electric fields on

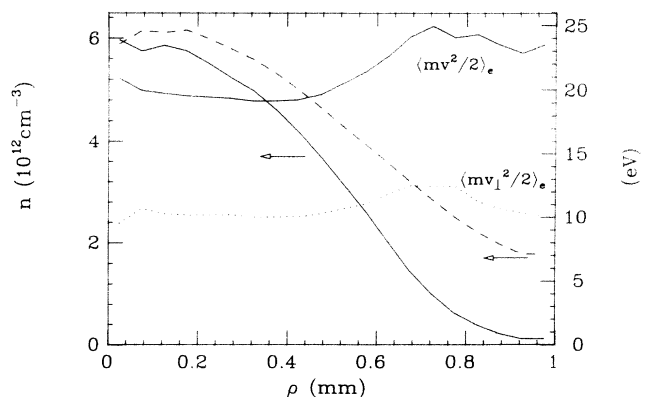


FIG. 4. Electron (solid) and ion (dashed) densities,  $\langle mv^2 \rangle_e$  (solid) and  $\langle mv^2_{\perp} \rangle_e$  (dots) as functions of  $\rho$ .

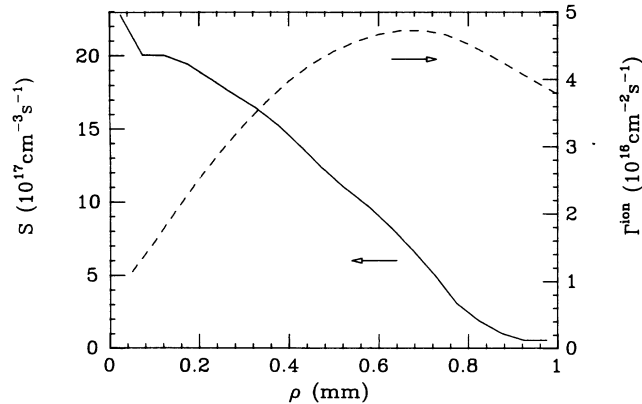


FIG. 5. Ion flux density  $\Gamma^{\text{ion}}$  (dashed) and ionization rate per unit volume  $S$  (solid) as functions of  $\rho$ .

electron transport coefficients. Their model is not actually a positive column model because it does not include wall losses. They assumed a parabolic radial potential. They were able to conclude that radial fields without wall losses have less influence on the total ionization rate than other phenomena such as multistep ionization.

Blank [15] explored the limits of the isothermal approximation for the electron energy distribution. He also used the venerable two-term Legendre expansion for the distribution. He assumed a constant electron-neutral elastic collision frequency which provided the dominant energy loss through recoil. A near Maxwellian distribution results from these assumptions. His approach is applicable to large radius-pressure products (low  $E/N$ ) with low current densities so that Coulomb collisions are negligible.

Tsendin [16] and Tsendin and Golubovskii [17] studied the effect of transverse or radial inhomogeneity in a positive column model. It is widely known that the electron energy distribution is depleted above the first inelastic threshold. Tsendin and Golubovskii found a second break in the electron distribution which can occur at the space charge potential of the positive column if the energy relaxation distance is large compared to the

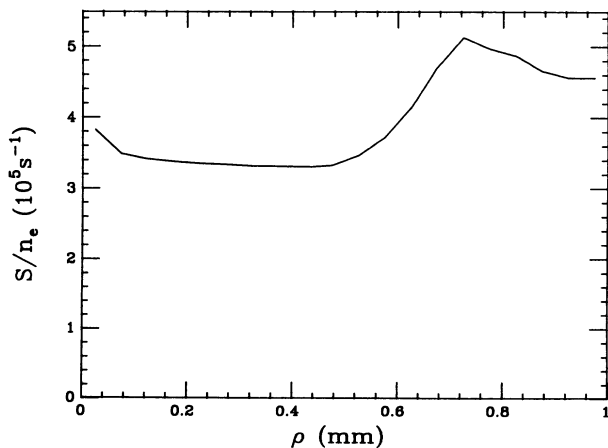


FIG. 6. Ionization rate ( $S/n_e$ ) as a function of  $\rho$ .

transverse dimensions of the column. This second break is a manifestation of diffusive cooling [18]. Diffusive cooling refers to a preferential loss of the tail of the electron distribution as energetic electrons climb the ambipolar potential to reach the positive column wall.

Zech *et al.* [19] reported a nonisothermal numerical model of a low pressure argon positive column under conditions comparable to those found in an argon ion laser. Their basic approach consisted of using established numerical methods to find simultaneous solutions of the fluid equations including coupled particle, momentum and energy conservation equations with Gauss's law. The relatively high electron density of  $2 \times 10^{14} \text{ cm}^{-3}$  in these simulations resulted in such a large electron thermal conductivity that no significant radial gradient of electron temperature was found.

Hartig and Kushner [20] recently described a positive column model based on a modified two-term Legendre expansion of the electron distribution function. The modification included the addition of energy resolved drift and diffusion as well as the effect of heating and/or cooling by the radial fields. Although their model is appropriate for larger radius-pressure products (low  $E/N$ ), their simulations did yield radial variations of average electron energy and ionization rates. They found an average electron energy that increases slightly with increasing radius, peaks, and then declines near the wall. They also found an ionization rate that decreases slightly with increasing radius. Hartig and Kushner explained their results as due to a competition between diffusive cooling and "Joule heating" in the ambipolar field. The competition between these phenomena affects different parts of the electron energy distribution differently; and thus changes the shape of the distribution with increasing radius. Diffusive cooling causes the decrease of the ionization rate (per electron) with increasing radius. Radial variations in the total (radial plus axial) electric field cause a radial variation in Joule heating and in the average electron energy in Hartig and Kushner's simulation [20]. Our simulation is yielding similar variations in the average electron energy shown in Fig. 4. Our simulation is for a small radius-pressure product (high  $E/N$ ) where inelastic collisions play a major role in the electron energy balance, and thus the energy relaxation distance is rather long in comparison to the column radius.

## VIII. CONCLUSION

We presented an accurate method for solution of the Boltzmann equation in the variables  $(\rho, v_z, v_\perp, \mathcal{M})$ . It was found that the moment arm or "reduced" angular momentum  $\mathcal{M}$  was an appropriate variable to describe the third component of the velocity with reduced numerical diffusion. Both ballistic and collision operators were described in detail. The ballistic mover for electrons was based on conservation of phase space volume and was shown to be physically correct in simple simulations. Preliminary results for a positive column were also reported. We will, in future work, compare radially resolved experimental results from a He positive column with a small radius-pressure product to these self-consistent kinetic

simulations. We will also in future work combine the previously reported method for the “planar” problem with variables  $(z, v_z, v_\perp)$  with the method reported here for the cylindrical problem with variables  $(\rho, v_z, v_\perp, \mathcal{M})$  to solve the Boltzmann equation in the variables  $(z, \rho, \vec{v})$ .

### ACKNOWLEDGMENT

This research is supported by the General Electric Company.

## APPENDIX: IMPLEMENTATION OF ANISOTROPIC COLLISIONS

### 1. Elastic collisions

Elastic collisions of electrons with neutral atoms are typically anisotropic in nature. A common assumption made by modelers of gas discharges is that use of the momentum transfer cross section is adequate. If this is used, the scattered electrons are redistributed isotropically in velocity space.

Instead, we here start with the differential cross section for elastic scattering. The differential cross section depends on the initial relative velocity between the electron and neutral atom and the angle through which the electron is scattered from its initial velocity. The azimuthal scattering angle is uniformly distributed, so we are only concerned with the polar angle  $\theta_s$ , to which the electron is scattered.

We first find the average cosine of the angle electrons scatter through, from the differential cross section,  $\overline{\cos \theta_s}$ . We also average over the cosine of the initial angle the electrons, which scatter to the same final speed ( $v'$ ), make with the  $z$  axis,  $\cos \theta_i$ . Then the average component of the final velocity along the  $z$  axis for the set of electrons is given by

$$\overline{v'_z} = \overline{\cos \theta_i} \overline{\cos \theta_s} v'. \quad (\text{A1})$$

This quantity, which is proportional to the average  $z$  momentum of electrons at speed  $v'$  after an elastic collision is used to redistribute the scattered electrons with an anisotropic distribution described in Sec. 3 of this appendix. Although the angular dependence of the scattering cross section is here approximated using a two-term Legendre polynomial, our approach could be modified for a multiterm expansion.

Since elastic collisions are an important collision process in the discharges considered here, it was shown [2,5] that special care must be taken to ensure numerical diffusion is minimized.

### 2. Inelastic collisions

Unlike elastic electron-neutral atom collisions, differential cross sections are not readily available for inelastic electron-neutral atom collisions. The lack of this information led us to introduce a parameter  $h$  which is the fraction of the maximum possible  $z$  momentum of the electron(s) which is conserved in inelastic collisions (including ionizing collisions).

Again, we start by considering electrons whose initial velocity makes an angle  $\theta_i$  with respect to the  $z$  axis. The average final velocity component along the  $z$  axis for this set of scattered electrons is given by

$$\overline{v'_z} = h \overline{\cos \theta_i} v'. \quad (\text{A2})$$

where  $h$  is a constant that represents the fraction of the available linear momentum of electron(s) that is conserved during inelastic collisions.

### 3. Implementation of angular distributions of scattered particles

We redistribute the electrons back onto the mesh using a two-term Legendre polynomial for the angular distribution, so that  $\overline{v'_z}$  and, of course, the number of electrons are conserved. The distribution of scattered electrons with respect to  $\mu (= \cos \theta)$  is  $f(\mu) = \frac{1}{2}(1 + \alpha\mu)$ . The first Legendre polynomial gives an isotropic distribution. It is now required to find the coefficient of the second polynomial  $\alpha$ . Conservation of  $\overline{v'_z}$  requires that

$$\overline{v'_z} = \frac{1}{2} \int_{-1}^1 v' \mu (1 + \alpha\mu) d\mu \quad (\text{A3})$$

(the factor of 1/2 is for normalization). Solving for  $\alpha$ , we find

$$\alpha = \frac{3\overline{v'_z}}{v'}. \quad (\text{A4})$$

The above redistribution becomes negative if  $|\alpha| \geq 1$ . If  $|\alpha| > 1$ , i.e.,  $|\overline{v'_z}/v'| > 1/3$ , we then restrict the range of  $\mu$  in which the electrons are redistributed so that both  $\overline{v'_z}$  and electron number can be conserved with a positive electron density. For  $\overline{v'_z} > 0$ , we let the lower limit of integration be  $\mu_l$ , and now use  $f(\mu) = 2(\mu - \mu_l)/(1 - \mu_l)^2$ . To determine  $\mu_l$  we require that  $\overline{v'_z}$  be conserved. We find

$$\mu_l = 3\overline{v'_z}/v' - 2. \quad (\text{A5})$$

In summary, if  $|\overline{v'_z}/v'| \leq 1/3$  then the electrons are redistributed using  $f(\mu) = \frac{1}{2}(1 + \frac{3\overline{v'_z}}{v'}\mu)$  over the full range of polar angles. Otherwise they are redistributed using  $f(\mu) = 2(\mu - \mu_l)/(1 - \mu_l)^2$  in a limited range of polar angles. Both cases conserve electron number and  $\overline{v'_z}$ .

As mentioned above a simplified version, which exactly conserves particles and energy on the mesh, of this full elastic scattering operator can be constructed [2,5].

- [1] G.J. Parker, W.N.G. Hitchon, and J.E. Lawler, J. Comput. Phys. **106**, 147 (1993).  
 [2] W.N.G. Hitchon, G.J. Parker, and J.E. Lawler, IEEE Trans. Plasma Sci. **21**, 228 (1993).

- [3] G.J. Parker, W.N.G. Hitchon, and J.E. Lawler, Phys. Lett. A **174**, 308 (1993).  
 [4] T.J. Sommerer, W.N.G. Hitchon, R.E.P. Harvey, and J.E. Lawler, Phys. Rev. A **43**, 4452 (1991).

- [5] W.N.G. Hitchon, G.J. Parker, and J.E. Lawler, IEEE Trans. Plasma Sci. **22**, 267 (1994).
- [6] F.F. Chen, *Introduction to Plasma Physics and Controlled Fusion* (Plenum Press, New York, 1984), Chap. 7.
- [7] R.W. LaBahn and J. Callaway, Phys. Rev. A **2**, 336 (1970); Phys. Rev. **180**, 91 (1969); **188**, 520 (1969).
- [8] G.D. Alkhazov, Zh. Tekn. Fiz. **40**, 97 (1970) [Sov. Phys. Tech. Phys. **15**, 66 (1970)].
- [9] S. Sinha, S.L. Lin, and J.N. Bardsley, J. Phys. B, **12**, 1613 (1979).
- [10] H. Helm, J. Phys. B, **10**, 3683 (1977).
- [11] J.E. Lawler, Phys. Rev. A, **22**, 1025 (1980).
- [12] W. Schottky, Z. Phys. **25**, 635 (1924).
- [13] L. Tonks and I. Langmuir, Phys. Rev. **34**, 876 (1929).
- [14] I.B. Bernstein and T. Holstein, Phys. Rev. **94**, 1475 (1954).
- [15] J.L. Blank, Phys. Fluids **11**, 1686 (1968).
- [16] L.D. Tsendin, Zh. Eksp. Teor. Fiz. **66**, 1638 (1974) [Sov. Phys. JETP **39**, 805 (1974)].
- [17] L.D. Tsendin and Yu. B. Golubovskii, Zh. Tekh. Fiz. **47**, 1839 (1977) [Sov. Phys. Tech. Phys. **22**, 1066 (1977)].
- [18] M.A. Biondi, Phys. Rev. **93**, 1136 (1954).
- [19] I. Zech, T. Ertl, H. Herold, H. Ruder, W.E. Kohler, and W. Tiemann, Contrib. Plasma Phys. **32**, 535 (1992).
- [20] M.J. Hartig and M.J. Kushner, J. Appl. Phys. **73**, 1080 (1993).